

Banner appropriate to article type will appear here in typeset article

Worthington Jets during Water Entry of Spheres with no Cavity Formed

Xingsheng Li¹ and Jing Li¹ †

¹Marine Numerical Experimental Center, State Key Laboratory of Ocean Engineering, School of Ocean and Civil Engineering, Shanghai Jiao Tong University, Shanghai 200240, China

(Received xx; revised xx; accepted xx)

Water entry problem has extensive applications in numerous areas of nature, industry, and science. Here, we investigate the Worthington jets generated during the water entry of solid spheres with no cavity formed experimentally and theoretically. Three different pinch-off modes are identified in experiments, which depend solely on the release height H and the diameter of the sphere D , regardless of the material of the sphere. A brief dimensional analysis of the experimental data indicates that the dimensionless maximum height of the jet h/D is proportional to the Froude number, defined as $Fr = 2H/D$. Based on the basic solution of flow past a sphere and the application of a reasonable potential function near the free surface, a theoretical model is developed diverging from the Rayleigh-Besant problem. Predictions regarding the shape and maximum height of the jet show good agreement with experimental results.

1. Introduction

Worthington jets generated during the free surface impact of solid or liquid objects have diverse beneficial applications, such as human Olympic diving (Rubin 1999), droplet manipulation (Klein *et al.* 2015), inkjet printing (van der Bos *et al.* 2014), and spray cooling and painting (Aziz & Chandra 2000). The importance of this phenomenon is also stressed as it can cause serious pesticide wasting (Nuruzzaman *et al.* 2016), air pollution (Landrigan *et al.* 2018), and even the spread of pollutants and pathogens (Joung & Buie 2015). Consequently, this entry problem has gained much attention since Worthington over a century ago (Worthington & Cole 1897). Extensive studies have examined various impact objects, including liquid droplets (Marcotte *et al.* 2019; Kim *et al.* 2021; Dong & Angeli 2023), spheres (Grumstrup *et al.* 2007; Duclaux *et al.* 2007; Aristoff & Bush 2009; Truscott *et al.* 2012; Speirs *et al.* 2019), and flat disks (Bergmann *et al.* 2006; Gekle *et al.* 2010; Gekle & Gordillo 2010). This jet has also been well investigated in the context of bubble bursting near the liquid surface (Lai *et al.* 2018; Kang & Cho 2019; Dubitsky *et al.* 2023).

After a solid body enters the water, considerable focus is given to the air entrainment circumstance. As the axisymmetric air cavity collapses due to hydrostatic pressure with a local scaling exponent $\alpha = d \ln h_0 / d \ln t'$ of the minimum radius h_0 of the cavity (Eggers *et al.* 2007), the pinch-off eventually happens in a single point and two jets are ejected upwards and downwards from this point, respectively (Gekle & Gordillo 2010). Through the theory of a

† Email address for correspondence: lijing_@sjtu.edu.cn

collapsing void, the upward Worthington jets have been proved to be fed by the local flow around the base of the jet, which is forced by the colliding cavity walls (Gekle *et al.* 2009). Usually, the Rayleigh–Plesset equation is effective and has been widely applied to model the collapse of the cavity (Duclaux *et al.* 2007; Aristoff & Bush 2009; Plesset & Prosperetti 1977). Among these studies, Aristoff & Bush (2009) presented a theoretical model to describe the evolution of cavity shape and obtained the analytical solution for pinch-off events, which shows excellent agreement with experiments. Furthermore, the boundary integral simulation provides another route for such cavity collapsing problem (Bergmann *et al.* 2009; Gekle & Gordillo 2010). Compared with the theoretical method which focuses on cavities, it gives more information about the jet.

However, in the absence of cavity formation during the entry process, the generation mechanism of the jet is entirely different. As shown in figure 1, upon impact the kinetic energy is transmitted directly to the fluid around the sphere, which is the primary source to support the generation of the jet. In this sense, traditional Rayleigh-Besant problem is not applicable anymore. Unlike the cavity collapsing forced jets, theoretical analysis on such no cavity formed entry problem is relatively limited. Existing research has just found that the maximum height of the jet is proportional to the release height from the perspective of energy (Watson *et al.* 2018), but parameters controlling the maximum height the jet can reach remain unclear.

In the current work, based on the experimental data across a wide range of parameters, we aim to find the factors affecting the evolution and pinch-off of the jet. Furthermore, we try to establish a novel theory based on potential flow theory to elucidate the generation mechanism of Worthington jets, which is verified by comparing with experiments.

2. Experimental description and qualitative observation

2.1. Experimental set-up and procedure

In our experiments, a sphere made of steel, aluminium, glass or polyoxymethylene(POM) with a diameter D is held by a pneumatic finger at a height of H above the free surface. The density ρ_s and contact angle θ_s of spheres made of different materials are listed in table 1. Each test is performed by releasing the sphere into a glass tank filled with water with dimensions of 0.5m×0.5m×0.5m. The impact velocity is estimated by $U_0 \approx \sqrt{2gH}$ under free fall motion. The evolution of the free surface is recorded using a high-speed camera at 400 frames/sec. To ensure the illumination intensity and quality of images, a light source combined with a diffuser screen is employed. Figure 1 illustrates the evolution of the jet after the sphere collides into water. Initially, when the sphere is completely submerged, a fine splash is first formed. After tens of milliseconds, this splash separates from the main liquid column and becomes tiny droplets. Because these splash and droplets in the early stage of the jet are sufficiently tiny, they are beyond the consideration of the jet shape and height.

2.2. Pinch-off modes

As the jet elongates rapidly in vertical direction, three different modes emerge depending on H . Figure 1(a) corresponds to a mode with no child droplet being disengaged from the main liquid column throughout the entire process of rising and falling. In contrast, a big child droplet is detached in the other two cases, indicating a pinch-off event. This phenomenon has been observed before in experiments of droplet impinging on a two-layer liquid and two pinch-off modes are identified depending on the location of the detachment of child droplets (Kim *et al.* 2021). Inspired by this, when a child droplet separates during the falling stage as shown in figure 1(b), the mode is termed “downward pinch-off”. In the opposite case (figure

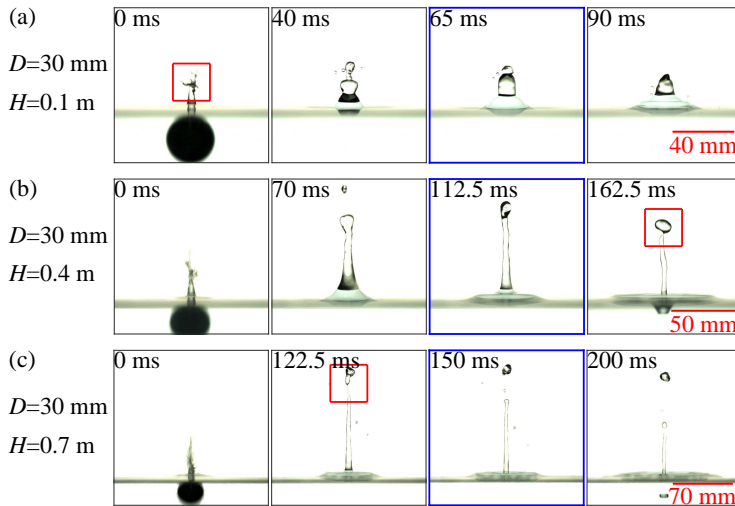


Figure 1: Image sequences of Worthington jets formed after steel spheres impact the free surface from various release heights. Each row corresponds to a series of experimental snapshots taken at different times. The snapshots framed in blue indicate the moment when the jet reaches its maximum height. The red rectangular box in (a) highlights the fine splash formed at the initial stage. The red rectangular boxes in (b) and (c) mark pinch-off of the liquid column.

Material	ρ_s (Kg/m ³)	θ_s (°)
Steel	7902	72 ± 2
Aluminium	2710	83 ± 3
Glass	2253	30 ± 1
Polyoxymethylene(POM)	1355	92 ± 2
Spheres coated with turtle wax super hard shell	/	103 ± 4

Table 1: Density ρ_s and contact angle θ_s of spheres made of different materials. The contact angle of spheres coated with turtle wax super hard shell is also listed.

1c), a child droplet has already formed before the jet reaches its maximum height, which is termed “upward pinch-off”. It should be stressed that even though the liquid column pinches off, the child droplet remains part of jet and is taken into account when it comes to the jet height and shape.

To highlight these pinch-off modes, we conduct experiments across a broader range of D and H utilizing spheres made of four different materials and identify their pinch-off positions. From figure 2(a-d), regardless of material, the regime diagrams of the jet exhibit similar patterns. When H is relatively small, the impact transmits less energy to the jet and there is not enough kinetic energy for the upper part of the jet to escape. As H increases, the jet acquires more kinetic energy which converges at the top. After the maximum height is reached, the lower part of the jet falls more quickly, and a child droplet forms under the action of surface tension. At a higher release height, the jet gains a greater initial speed, causing the upper part to rise faster and separate from the lower part. Additionally, the volume of the jet is approximately proportional to the volume of the sphere (Watson *et al.* 2018), which means more kinetic energy is needed for the jet to pinch off as D increases.

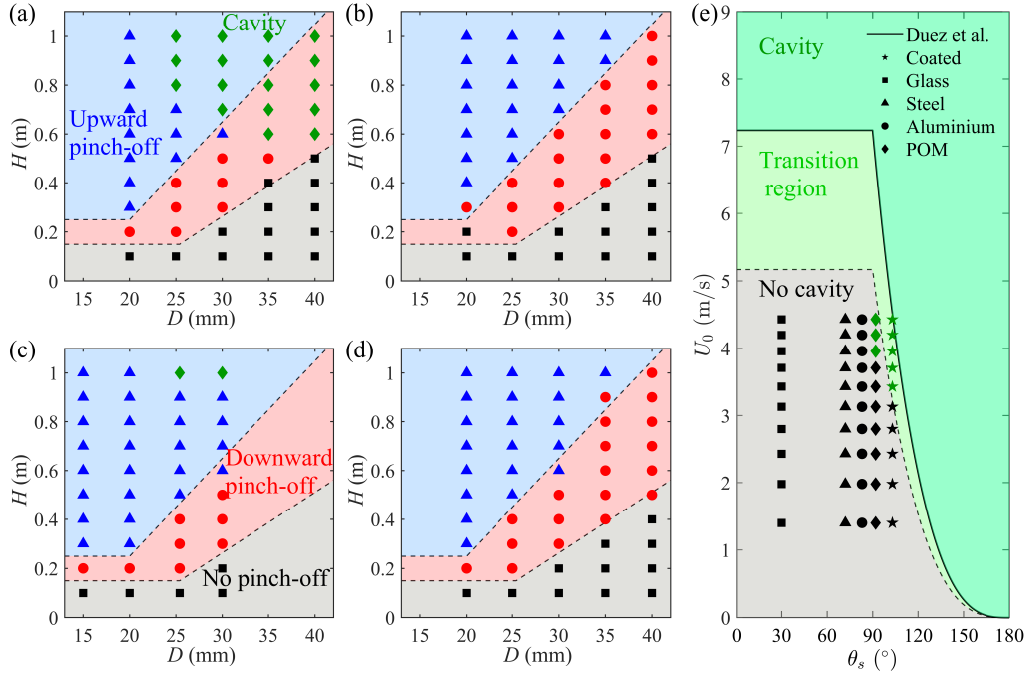


Figure 2: (a-d) Regime diagrams illustrating the pinch-off modes of Worthington jets corresponding to spheres made of POM, glass, aluminium, and steel, respectively. Squares: no pinch-off happening; circles: pinch-off happening during the falling stage; triangles: pinch-off happening during the rising stage; diamonds: cavity formed cases. The regime separation lines are least-square fitted from the midpoints between two adjacent modes. Each dot corresponds to at least 3 repeated tests. (e) Impact velocity for cavity formation versus contact angle θ_s . Squares, triangles, circles, diamonds, and stars denote experimental results for spheres made of glass, steel, aluminium, POM, and spheres coated with turtle wax super hard shell made of arbitrary materials mentioned above, respectively. Diameter of the sphere is not shown explicitly. The solid line corresponds to the theoretical curve given by Duez *et al.* (2007). The dashed boundary is obtained by changing parameters in their mathematical model to fit the present experiments.

Apart from three different pinch-off modes, cavity may appear for POM spheres (figure 2a). Duez *et al.* (2007) gave the critical velocity for air entrainment depending on the contact angle of the impacting body, which is plotted together with the current experimental data in figure 2(e). For hydrophilic spheres (figure 2b-d), the critical velocity for cavity formation is identical and far beyond the impact velocity in our experiments. But for hydrophobic spheres, this critical velocity decreases nonlinearly with increased θ_s , which means it is more likely to be achieved in experiments on POM spheres (figure 2a). It is worth noting that POM spheres can create cavities at a velocity lower than the theoretical one. To explain this observation, we expand the experimental data in hydrophobic cases by coating spheres with turtle wax super hard shell (Speirs *et al.* 2019), which leads to $\theta_s = 103 \pm 4^\circ$. By changing parameters in the mathematical model given by Duez *et al.* (2007) to fit the present experiments, the dashed boundary from cavity formed to no cavity formed states is obtained. Obviously, there is a transition state between this critical boundary and the theoretical curve obtained from Duez *et al.* (2007) marked in light green in figure 2(e). This mixed region is also found by Truscott & Techet (2009) and is attributed to the effect of roughness.

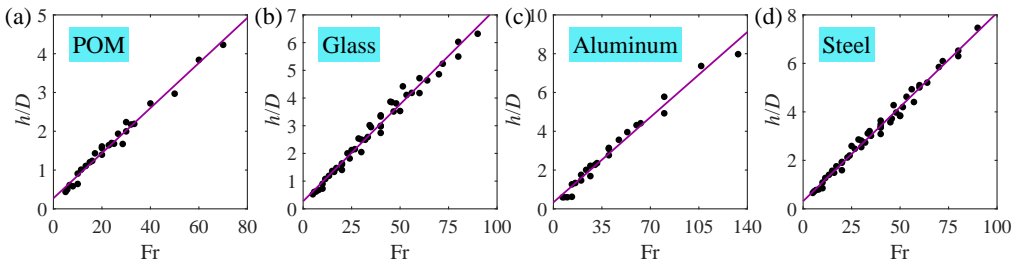


Figure 3: Dimensionless maximum height of the jet h/D against Fr . Black points represent experimental results, while solid lines correspond to the linear relationship between h/D and Fr fitted from experimental data.

3. Theoretical analysis

3.1. Dimensional analysis

Now that the geometric features of the jet are clarified qualitatively, we proceed to a quantitative analysis. With a comprehensive set of experimental data, dimensional analysis provides a direct and effective method to relate the maximum height of the jet h to the following experimental parameters: the density and diameter of the sphere ρ_s and D , the impact velocity U_0 , gravitational acceleration g , contact angle of the sphere with water θ_s , kinetic viscosity ν , surface tension coefficient σ and density ρ_w of water. By non-dimensionalizing with D , ρ_w , and g , the relationship between h and the above parameters can be expressed as

$$\frac{h}{D} = f\left(Fr, We, Re, \frac{\rho_s}{\rho_w}, \theta_s\right), \quad (3.1)$$

where $Fr = 2H/D$, $We = 2gH\rho_w D/\sigma$, and $Re = \sqrt{2gHD}/\nu$ are Froude, Weber, and Reynolds numbers, respectively. In the range of our experiments, the Reynolds number $Re > O(10^5)$ is sufficiently large to render the effect of viscosity negligible. The dimensionless number ρ_s/ρ_w reflects the density ratio between the sphere and water, which is bonded with θ_s together for spheres made of the same material. Because these two factors cannot be controlled independently in experiments, they are excluded from our dimensional analysis for simplicity.

Assuming $h/D \propto Fr^\alpha We^\beta$, we can expand it as $h \propto H^{\alpha+\beta} D^{-\alpha+\beta+1} (g\rho_w/\sigma)^\beta$. From experimental results, keeping D fixed, h increases linearly with H , while h remains nearly constant when D varies. These observations lead to the mathematical relationships $\alpha + \beta = 1$ and $-\alpha + \beta + 1 = 0$ which are solved to yield a scaling law for the dimensionless maximum height of the jet such that $h/D \propto Fr$.

In figure 3, the experimental data show an excellent agreement with this scaling law. Variations in the slope of the linear curves for spheres made of different materials may be attributed to differences in density and contact angle, which requires further refined experiments to uncover.

3.2. Mathematical model

After the brief dimensional analysis, a more detailed exploration based on potential flow theory may be efficient to reveal the generation mechanism of the jet. For such axisymmetric liquid columns, cylindrical coordinates are utilized, where z is set along the upward direction with $z = 0$ representing the free surface at rest, and r is along the radial direction. In the Rayleigh-Besant problem, the velocity field is expressed by radial velocity of the cavity walls to model the expansion of cavity (Aristoff & Bush 2009). Nevertheless, the jet considered

here is slender and extends mainly vertically, thus only the vertical velocity component is retained, which can be simplified to be a function of the vertical direction only (Che & Matar 2018). Considering that the velocity field should satisfy the kinematic boundary condition at $z = \eta$ and the value should decay along the negative z -direction, we assume the velocity distribution to be $w(r, z, t) = e^{(z-\eta)/\sqrt{DH}} \partial_t \eta$, where $\eta(r, t)$ denotes the position of the free surface. Specially, we use \sqrt{DH} to complete the non-dimensionalizing process, which characterizes the volume and speed of the jet. This introduction makes sense due to the experimental observations that a larger D results in a larger jet and a higher H correlates with a higher impact velocity and a higher h . Consequently, the velocity potential is expressed as

$$\phi(r, z, t) = \sqrt{DH} e^{(z-\eta)/\sqrt{DH}} \partial_t \eta. \quad (3.2)$$

Then, we apply the dynamic boundary condition $\partial_t \phi + w^2/2 = -g\eta$ at the free surface. By substituting the expressions for ϕ and w into it, we obtain an equation governing the evolution of $\eta(r, t)$:

$$\frac{\partial^2 \eta}{\partial t^2} = \left[\frac{1}{2} \left(\frac{\partial \eta}{\partial t} \right)^2 - g\eta \right] / \sqrt{DH}. \quad (3.3)$$

From the dimensional analysis, h/D is independent of We , indicating that the effect of surface tension on the development of the jet is negligible. This conclusion is also corroborated by incorporating a term $\sigma/\rho_w (\partial_{rr} \eta + \partial_r \eta/r)$ into the dynamic boundary condition, which gives nearly the same results as (3.3). Hence, the surface tension is neglected in the proposed theory.

By now, a mathematical description of the jet has been established. To make this model solvable, initial conditions must be specified. Because the center of the sphere is located at $z = -D/2$ when $t = 0$, and the surface is still flat ignoring the fine splash as shown in figure 1, we set

$$\eta = 0, \quad \text{at } t = 0 \quad (3.4)$$

as an initial condition.

Since no cavity is formed in this problem and energy is transmitted to the fluid around the sphere upon impact, the initial velocity of the jet $\partial_t \eta$ is determined by the flow field around the sphere. In the absence of the free surface, the flow field is obtained from the basic solution of flow past a sphere, where the velocity potential of the flow near the sphere is given by $\phi_s = -D^3 U(t) [z - Z(t)] / 16 [r^2 + (z - Z(t))^2]^{3/2}$ in the present cylindrical coordinates with $Z(t)$ and $U(t)$ denoting the vertical position and sinking speed of the sphere, respectively. Because experimental snapshots indicate that the change in $U(t)$ before and after impact is slight, we set $U(0) = -U_0$ and $Z(0) = -D/2$. The velocity profile of the fluid following the sphere at $z = 0$ when $t = 0$ is then derived by taking z -derivative of ϕ_s , which reads

$$u_0(r) = \frac{D^3 U_0 (r^2 - D^2/2)}{16 (r^2 + D^2/4)^{5/2}}. \quad (3.5)$$

When the free surface is taken into account, an equation connecting u_0 with $\partial_t \eta$ is the law of conservation of momentum at the moment just before and after impact

$$-\pi \rho_s D^3 U_0 / 6 = \pi \rho_s D^3 U(0) / 6 + \rho_w V_w u_0 + \rho_w V_j \partial_t \eta. \quad (3.6)$$

In this equation, the volumes of the jet and the fluid following the sphere have the same magnitude: $V_j \sim V_w \sim \pi D^3 / 6$. Thus, we approximate $\partial_t \eta \sim u_0$ and assume that $\partial_t \eta = -c_0 u_0$. The value of c_0 is challenging to be accurately calculated from the momentum conservation

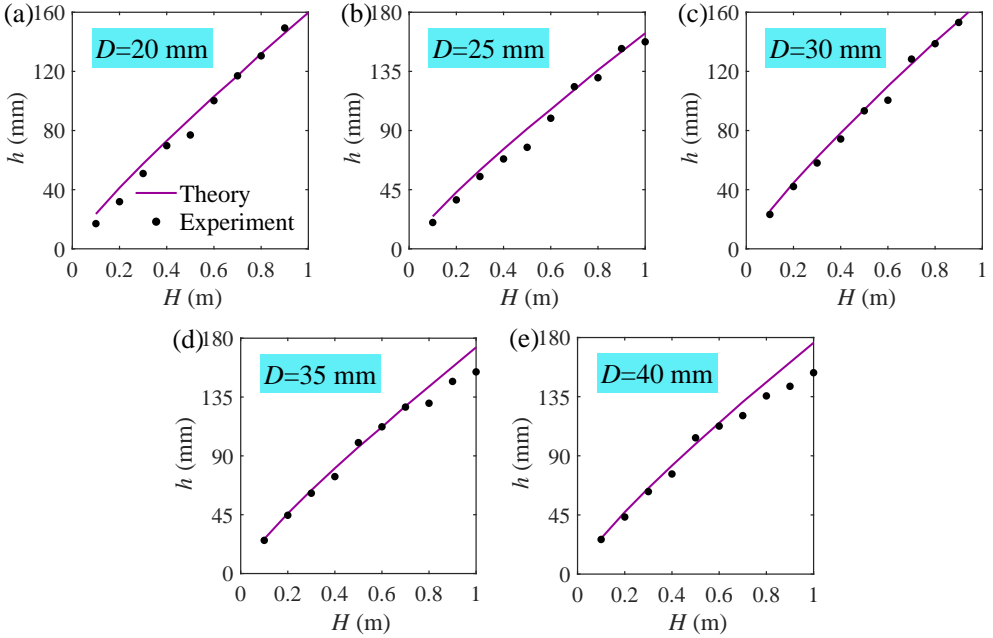


Figure 4: Maximum height of the jet generated during the water entry of steel spheres. Experimental data (solid points) and theoretical results (solid lines) are compared for various H and D .

equation (3.6) due to the difficulty in measuring V_j and V_w experimentally. To determine c_0 , we randomly select an experimental case and solve (3.3) numerically to obtain the maximum height of the jet. Fitting it with experimental data leads to $c_0 = 0.21$, a value consistent across all experimental cases for steel spheres. Actually, this value is reasonable since the volume of the jet is approximately equal to that of the sphere and $V_w < V_j$. The initial condition for $\partial_t \eta$ is summarized as

$$\partial_t \eta = -\frac{0.21 D^3 U_0 (r^2 - D^2/2)}{16 (r^2 + D^2/4)^{5/2}}, \quad \text{at } t = 0. \quad (3.7)$$

Together with (3.4) and (3.7), equation of $\eta(r, t)$ (3.3) is solved numerically.

4. Results and discussion

4.1. Maximum height of the jet

From figure 4, within the range of experimental parameters, the above theory agrees well with experiments. The theory successfully predicts the trend of h increasing linearly with H , and is effective for arbitrary D . However, influence of the density of spheres is not considered by now. According to experimental observations, differences in density or material result in different amounts of momentum being transmitted to the jet during the impact process, which is reflected in that spheres with higher densities tend to produce higher jet heights. This factor can be incorporated into the theory through momentum conservation equation (3.6), where different ρ_s may result in different values of c_0 . But we have assumed that $U(0) = -U_0$, which means that ρ_s is eliminated in that equation. To introduce the effect of differences in

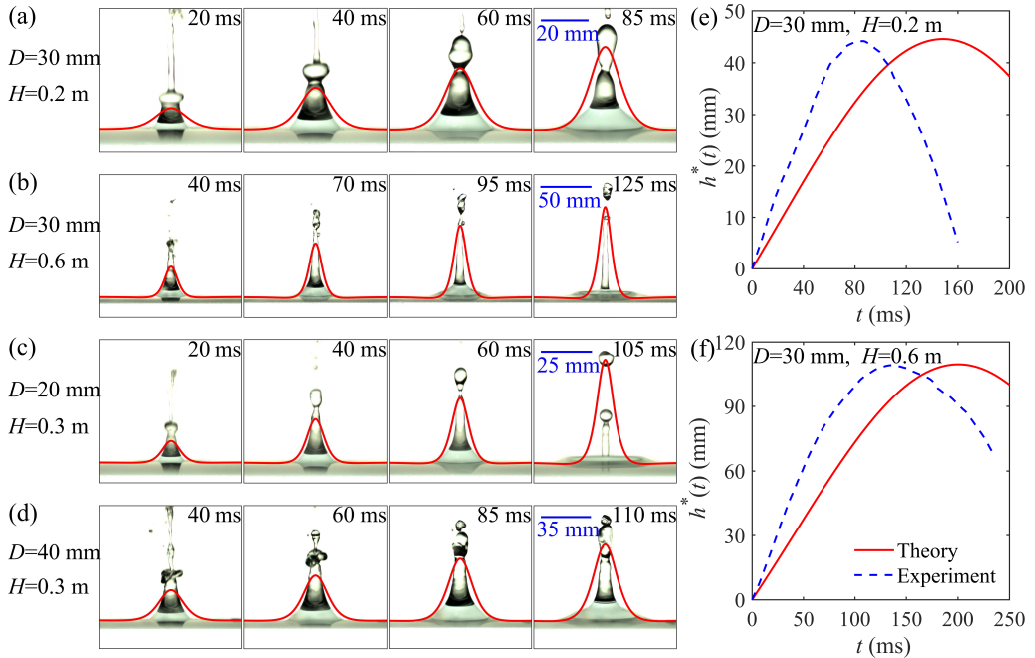


Figure 5: (a-d) Image sequences of experimental snapshots alongside the corresponding theoretical results. The impact objects are steel spheres. Each row corresponds to a series of experimental snapshots taken at different times. Red solid lines represent the theoretical results extracted at the same time as the corresponding experimental snapshots. (e-f) Evolution of the jet height $h^*(t)$ obtained from the present theory (solid lines) and its comparison with experimental results (dashed lines).

material, this assumption should be modified, which falls outside the interest of the present study.

4.2. Jet shape

In addition to the prediction on the maximum height, the theory also provides insights into the evolution of the jet shape. Figure 5(a-d) illustrates that the present theory successfully captures the variation in jet shape with respect to both D and H . This agreement becomes more apparent for the lower part of the jet, where the theoretical predictions align well with experimental observations.

For higher H (figure 5b), the jet is more slender due to the increased rising speed and greater jet height. Similarly, for smaller spheres (figure 5c), the jet is more slender due to the reduced jet volume. In these cases, the outlines given by theory are wider and lower than the experimental ones, especially in the later stage of the jet. To clarify the deviation of the developed theory, we plot the height of the jet over time $h^*(t)$ in figure 5(e-f). Results show that there is a time lag between theory and experiment, indicating that present theory predicts a slower jet velocity compared with experiments. Taking the same moment, the theoretical jet height is lower than the experimental one, which coincides with results shown in figure 5(a-d). Che & Matar (2018) once studied the evolution of jet height from the aspect of energy. With the assumption of a linear velocity distribution, the variation of jet height over time fits experimental results well. However, information about the jet shape cannot be obtained, and the total energy must be given in advance, which completely depends on the

experiment in the final stage of the jet. In this sense, present theory shows an advantage in the prediction of jet shape.

Actually, a bell-shaped profile for the jet has been assumed in our theory, which is incorporated into the initial condition (3.7). But our experiments reveal that the jet undergoes the process of elongation and pinch-off, which may result in a higher velocity for the upper part of the jet. This phenomenon cannot be simulated by the bell-shaped assumption. As a result, while the theory gives a good description about the volume which reflects the total energy of the jet, it cannot catch the accumulation of fluid at the top of the jet, leading to the discrepancy in the evolution of jet shape and height. To address this limitation, more attention should be paid to the secondary flow in the jet.

5. Conclusions

Compared with cavity collapsing forced Worthington jets, the jet generated during water entry of solid spheres with no cavity formed has obtained less attention. In this paper, we have validated that the generation of such jets is driven by the energy transmitted to the fluid around the sphere at the initial moment of impact. Once the jet forms, its pinch-off is controlled by the release height and the size of the sphere, regardless of the wettability and density of the sphere. Through a dimensional analysis, the mathematical relationship between the maximum height of the jet and experimental parameters is obtained that $h/D \propto Fr$. Also, we find that the effects of viscosity and surface tension on the development of the jet are negligible. A novel mathematical model based on potential flow theory is then established, whose results on the jet shape and maximum height agree well with experiments. These insights may advance the study of water entry problem and be beneficial to the application in industry, environment, and human activity.

Considering that the bell-shaped assumption cannot model elongation and pinch-off of the jet, present theory predicts a slower rising velocity than experiments. The secondary flow in the jet might result in the discrepancy between theory and experiment, which deserves more attention to improve the current theory.

Acknowledgements. The authors thank Yufei Zhang, Xue Jiang, and Mengyuan Jin for their preliminary work on this paper.

Funding. This work was supported by the Fundamental Research Funds for the Central Universities.

Declaration of interests. The authors report no conflict of interest.

REFERENCES

- ARISTOFF, JEFFREY M & BUSH, JOHN WM 2009 Water entry of small hydrophobic spheres. *Journal of Fluid Mechanics* **619**, 45–78.
- AZIZ, SHIRAZ D. & CHANDRA, SANJEEV 2000 Impact, recoil and splashing of molten metal droplets. *International Journal of Heat and Mass Transfer* **43** (16), 2841–2857.
- BERGMANN, RAYMOND, VAN DER MEER, DEVARAJ, STIJNMAN, MARK, SANDTKE, MARIJN, PROSPERETTI, ANDREA & LOHSE, DETLEF 2006 Giant bubble pinch-off. *Physical review letters* **96** (15), 154505.
- BERGMANN, RAYMOND, VAN DER MEER, DEVARAJ, GEKLE, STEPHAN, VAN DER BOS, ARJAN & LOHSE, DETLEF 2009 Controlled impact of a disk on a water surface: cavity dynamics. *Journal of Fluid Mechanics* **633**, 381–409.
- VAN DER BOS, ARJAN, VAN DER MEULEN, MARK-JAN, DRIESSEN, THEO, VAN DEN BERG, MARC, REINTEN, HANS, WIJSHOFF, HERMAN, VERSLUIS, MICHEL & LOHSE, DETLEF 2014 Velocity profile inside piezoacoustic inkjet droplets in flight: Comparison between experiment and numerical simulation. *Phys. Rev. Appl.* **1**, 014004.
- CHE, ZHIZHAO & MATAR, OMAR K 2018 Impact of droplets on immiscible liquid films. *Soft Matter* **14** (9), 1540–1551.

- DONG, TENG & ANGELI, PANAGIOTA 2023 Pinching dynamics and multiple droplet generation in partial coalescence. *Physical Review Letters* **131** (10), 104001.
- DUBITSKY, LENA, McRAE, OLIVER & BIRD, JAMES C 2023 Enrichment of scavenged particles in jet drops determined by bubble size and particle position. *Physical Review Letters* **130** (5), 054001.
- DUCLAUX, V, CAILLÉ, F, DUEZ, C, YBERT, C, BOCQUET, L & CLANET, C 2007 Dynamics of transient cavities. *Journal of Fluid Mechanics* **591**, 1–19.
- DUEZ, CYRIL, YBERT, CHRISTOPHE, CLANET, CHRISTOPHE & BOCQUET, LYDERIC 2007 Making a splash with water repellency. *Nature physics* **3** (3), 180–183.
- EGGERS, J, FONTELOS, MA, LEPPINEN, D & SNOEIJER, JH 2007 Theory of the collapsing axisymmetric cavity. *Physical review letters* **98** (9), 094502.
- GEKLE, STEPHAN & GORDILLO, JOSÉ MANUEL 2010 Generation and breakup of worthington jets after cavity collapse. part 1. jet formation. *Journal of fluid mechanics* **663**, 293–330.
- GEKLE, STEPHAN, GORDILLO, JOSÉ MANUEL, VAN DER MEER, DEVARAJ & LOHSE, DETLEF 2009 High-speed jet formation after solid object impact. *Physical review letters* **102** (3), 034502.
- GEKLE, STEPHAN, PETERS, IVO R, GORDILLO, JOSÉ MANUEL, VAN DER MEER, DEVARAJ & LOHSE, DETLEF 2010 Supersonic air flow due to solid-liquid impact. *Physical review letters* **104** (2), 024501.
- GRUMSTRUP, TORBEN, KELLER, JOSEPH B & BELMONTE, ANDREW 2007 Cavity ripples observed during the impact of solid objects into liquids. *Physical review letters* **99** (11), 114502.
- JOUNG, YOUNG SOO & BUIE, CULLEN R 2015 Aerosol generation by raindrop impact on soil. *Nature communications* **6** (1), 6083.
- KANG, YOUNG J & CHO, YEUNWOO 2019 Gravity–capillary jet-like surface waves generated by an underwater bubble. *Journal of Fluid Mechanics* **866**, 841–864.
- KIM, DOHYUNG, LEE, JINSEOK, BOSE, ARIJIT, KIM, ILDOO & LEE, JINKEE 2021 The impact of an oil droplet on an oil layer on water. *Journal of Fluid Mechanics* **906**, A5.
- KLEIN, ALEXANDER L., BOUWHUIS, WILCO, VISSER, CLAAS WILLEM, LHUISSIER, HENRI, SUN, CHAO, SNOEIJER, JACCO H., VILLERMAUX, EMMANUEL, LOHSE, DETLEF & GELDERBLUM, HANNEKE 2015 Drop shaping by laser-pulse impact. *Phys. Rev. Appl.* **3**, 044018.
- LAI, CHING-YAO, EGGERS, JENS & DEIKE, LUC 2018 Bubble bursting: universal cavity and jet profiles. *Physical review letters* **121** (14), 144501.
- LANDRIGAN, PHILIP J, FULLER, RICHARD, ACOSTA, NEREUS JR, ADEYI, OLUSOJI, ARNOLD, ROBERT, BALDÉ, ABDOULAYE BIBI, BERTOLLINI, ROBERTO, BOSE-O'REILLY, STEPHAN, BOUFFORD, JO IVEY, BREYSSE, PATRICK N & OTHERS 2018 The lancet commission on pollution and health. *The lancet* **391** (10119), 462–512.
- MARCOTTE, FLORENCE, MICHON, GUY-JEAN, SÉON, THOMAS & JOSSERAND, CHRISTOPHE 2019 Ejecta, corolla, and splashes from drop impacts on viscous fluids. *Physical review letters* **122** (1), 014501.
- NURUZZAMAN, MD., RAHMAN, MOHAMMAD MAHMUDUR, LIU, YANJU & NAIDU, RAVI 2016 Nanoencapsulation, nano-guard for pesticides: A new window for safe application. *Journal of Agricultural and Food Chemistry* **64** (7), 1447–1483.
- PLESSET, MILTON S & PROSPERETTI, ANDREA 1977 Bubble dynamics and cavitation. *Annual review of fluid mechanics* **9**, 145–185.
- RUBIN, BENJAMIN D 1999 The basics of competitive diving and its injuries. *Clinics in sports medicine* **18** (2), 293–303.
- SPEIRS, NATHAN B, MANSOOR, MOHAMMAD M, BELDEN, JESSE & TRUSCOTT, TADD T 2019 Water entry of spheres with various contact angles. *Journal of Fluid Mechanics* **862**, R3.
- TRUSCOTT, TADD T, EPPS, BRENDEN P & TECHET, ALEXANDRA H 2012 Unsteady forces on spheres during free-surface water entry. *Journal of Fluid Mechanics* **704**, 173–210.
- TRUSCOTT, TADD T & TECHET, ALEXANDRA H 2009 A spin on cavity formation during water entry of hydrophobic and hydrophilic spheres. *Physics of Fluids* **21** (12).
- WATSON, DAREN A., STEPHEN, JEREMY L. & DICKERSON, ANDREW K. 2018 Jet amplification and cavity formation induced by penetrable fabrics in hydrophilic sphere entry. *Physics of Fluids* **30** (8), 082109.
- WORTHINGTON, ARTHUR MASON & COLE, REGINALD SORRÈ 1897 V. impact with a liquid surface, studied by the aid of instantaneous photography. *Philosophical Transactions of the Royal Society of London. Series A, Containing Papers of a Mathematical or Physical Character* **189** (189), 137–148.